Evaluation of antilock braking system with an integrated model of full vehicle system dynamics

T.K. Bera **K. Bhattacharya** **A.K. Samantaray***

Department of Mechanical Engineering, Indian Institute of Technology, 721302 Kharagpur, India.

ABSTRACT

Antilock braking system (ABS), traction control system *etc.* are used in modern automobiles for enhanced safety and reliability. Autonomous ABS system can take over the traction control of the vehicle either completely or partially. An antilock braking system using an on-off control strategy to maintain the wheel slip within a predefined range is studied here. The controller design needs integration with the vehicle dynamics model. A single wheel or a bicycle vehicle model considers only constant normal loading on the wheels. On the other hand, a four wheel vehicle model that accounts for dynamic normal loading on the wheels and generates correct lateral forces is suitable for reliable brake system design. This paper describes an integrated vehicle braking system dynamics and control modelling procedure for a four wheel vehicle. The vehicle system comprises several energy domains. The interdisciplinary modelling technique called bond graph is used to integrate models in different energy domains and control systems. The bond graph model of the integrated vehicle dynamic system is developed in a modular and hierarchical modeling environment and is simulated to evaluate the performance of the ABS system under various operating conditions.

Keywords: Bond graph, antilock braking system, vehicle dynamics.

1. Introduction

The main motivating factor behind this work on vehicle dynamics and antilock braking systems are the conditions that prevail in Indian roads, especially in sub-urban, semi-urban and rural areas, where road infrastructure is poor and traffic is chaotic. The vehicle performance is severely challenged in these conditions and optimizing the

* Corresponding author: Tel: +91 3222 282998/282999, Fax: +91 3222 282277
E-mail: samantaray@lycos.com; ak_samantaray@yahoo.com; samantaray@mech.iitkgp.ernet.in

performance of the mechatronic systems require controllers to be tuned by trial and error through exhaustive simulations and field testing. This is why Indian automobile industry has been very conservative in adopting modern technology. The ABS is to be designed for diverse driving conditions, especially where frequent braking and acceleration is required. Thus, increasing the life of the braking system in these conditions becomes important.

Nomenclature

a	Distance of front axle from the vehicle cg	τ	Torque
A	Area	σ	Slip ratio
b	Distance of rear axle from vehicle cg	μ	Coefficient of friction
B	Stiffness factor	μ_{m}	Motor torque constant
c	Half of track width		
C	Shape factor		
		Subscripts	
C_1	Maximum value of friction curve	a	Arm
C_2	Friction curve shape	b	Braking
C_3	Friction coefficient difference between the maximum value and value at $\sigma_{\mathrm{x}} = 1$	bc	Brake cylinder
C_4	Wetness characteristic value	bd	Brake drum
D	Peak value	c	Vehicle body
E	Curvature factor	cfr, crr	Front and rear cornering force
F	Force	ca	Cable
h	Height of vehicle cg from suspension reference point	cx, cy, cz	x , y, z–direction of vehicle body
J	Polar moment of inertia	e	Equivalent
K	Stiffness	E	Engine
k_g	Discontinuous controller gain	fr	Front
l	Length	l	Left
m	Mass	lm	Mechanical loss
M	Moment	m	motor
r	Effective radius	nfr, nrr	Normal for front and rear wheel
R	Damping	r	Right
S	Sliding surface	re	Return
V	Volume	rr	Rear
$v, \boldsymbol{V}$	Velocity, Velocity vector	stx, sty, stz	x, y, z direction of structure
x, y, z	Displacements in three directions	st	Steering (front axle)
$\dot{x}, \dot{y}, \dot{z}$	Velocities in three directions	stw	Steering wheel
$\ddot{x}, \ddot{y}, \ddot{z}$	Accelerations in three directions	sx, sy, sz	x, y, z direction of suspension
x_{o}	Output variable	t	Tyre
y_{i}	Input variable	tfr, trr	Tangential (front and rear)
α	Lateral slip angle	v	Vehicle
γ	Camber angle	w	Wheel
δ	Steering angle	wx, wy, wz	x, y, z direction of wheel
$\dot{\theta}, \ddot{\theta}$	Angular velocity, acceleration	1	Left suspension reference point

Modelling and simulation of physical phenomena and physical systems plays a very important role in understanding the underlying science. The necessary steps involved in modelling are writing the equations for each elementary physical system, sorting these equations and implementing them in a solver. This approach becomes time-consuming when the system becomes complex and multidisciplinary in nature. A common tool enabling a unified approach to the physical modelling of various disciplines is bond graph [1– 4]. Bond graph technique is also well suited for modular modelling of large physical systems. A vehicle dynamic system is a multi-energy domain system which involves mechanical, hydraulic, pneumatic, electronic, electrical, chemical (batteries or fuel cells), thermal domains, to name a few. Bond graph modeling is an ideal tool to develop an integrated model of such a system with coupling of several energy domains. Multi bond graph is suitable for compact representation of complex multibody system models [5, 6]. Moreover, efficient control algorithms can be derived from analysis of the bond graph structure [7–10]. For the above reasons, bond graph models have been extensively used for design of mechatronic systems [1, 11, 12]. Although this article concerns only a few energy domains, bond graph modeling has been used here to keep open the possibilities for addition of further dynamical component models (*e.g.*, IC engine, electric motor drive, fuel cell, transmission system, *etc.*).

Bond graph modelling has been extensively used in vehicle dynamics studies [13, 14]. A four-wheel, nonlinear vehicle dynamic model with electrically controlled brakes and steering was developed by Margolis and Shim [15]. Three dimensional dynamics of coupled bodies and the multiple transformations required to model multibody systems were developed by Pacejka [16]. The engine model along with drive train and vehicle dynamics models with complexity was developed by Louca *et al.* [17]. In this paper, initially, a bicycle model with steering is considered for basic brake system design. Then a full vehicle model which has 6-DOF for the vehicle chassis and 6-DOF for each wheel and includes tyre forces [18] is used to study the vertical, longitudinal and lateral vehicle dynamics. Bond graph model for the braking system is then integrated with the vehicle model for dynamic analysis.

Antilock braking system (ABS) is an electronically controlled braking system that maintains control over the directional stability of the vehicle during emergency braking or braking in slippery road by preventing the wheel lock-up. Another advantage of using ABS is reduction in the stopping distance during emergency braking or braking in slippery road. This is achieved by utilizing the maximum brake power available for which the wheel does not get locked [19]. However soft surfaces or surfaces made up of gravels can enhance stopping distances. Conventional ABS has some limitations in control and performance. One main drawback of conventional ABS is the slip control

strategy where the slip is maintained in an acceptable range [20] rather than at the optimal value. Friction forces generated during vehicle acceleration or braking are proportional to the normal load on the wheels of the vehicle. Studies show that the friction co-efficient is a nonlinear function of the wheel slip [21]. ABS controller is developed to keep the vehicle slip in a particular range for which the road wheel friction coefficient is highest, to achieve optimal performance. Obtaining an accurate mathematical model of ABS is very difficult as the controller operates in an unstable equilibrium point. It is also very difficult to identify the actual road surface by using any available sensor and then to use those data in optimizing the ABS controller performance. Various control algorithms such as sliding mode control [22], fuzzy logic [23], and neural networks are reported in literature to optimize the ABS performance.

One finds several articles in literature dealing with quarter car ABS models. However, the quarter car model is unsuitable to evaluate ABS performance during a curve negotiation. This necessitates the use of a bicycle model of the vehicle where steering or handling model is included. Although the bicycle model offers improved response characteristics than the single wheel model, it does not represent the true dynamics of the ABS equipped vehicle. When a vehicle brakes, the vehicle tilts forward and the load shifts from the rear wheels to the front wheels. The reverse happens when the vehicle accelerates. Likewise, during a turn, the vehicle load is transferred from the inner wheels to the outer wheels. The peak ABS braking force depends on the value of the coefficient of friction between the tire and the ground, which in turn depends on the normal load on the tire and other factors. Thus, proper accounting of the load transfer is required to accurately predict the ABS system performance. The load transfer mechanism during braking and turning cannot be represented in the bicycle model. Therefore, a four wheel vehicle model should be used for final performance evaluation, although the single wheel and bicycle models may be used in the initial design stage.

The structure of this paper is as follows: First, models of various subsystems of the full vehicle model are explained along with the control algorithms for ABS. Then the detailed bond graphs of bi-cycle model and full vehicle model are constructed based on the various kinematic relations. Finally, simulation results of vehicle dynamics along with antilock braking system are provided and compared.

2. Brake System Model

The wheels are modelled by their mass, rotary inertia, radius and tyre stiffness. Tyre is the most important among wheel components because tyre forces and moments play an important role in vehicle dynamics. Tyre forces are

necessary to control the vehicle. As the tyres are the only means of contact between the road and the vehicle, they are the key factors determining the vehicle handling performance. Tyre models are broadly classified as physical models, analytical models, and empirical models. The physical models are constructed to predict tyre elastic deformation and tyre forces [25]. In such models, complex numerical methods are required to solve the equations of motion. Analytical models are not useful at large slip and at combined slip. Empirical models based on experimental correlations are generally more accurate [26]. Pacejka's *magic formula* [18] is a widely used empirical model with which one can compute the longitudinal and cornering forces and self aligning moment.

2.1. Tyre slip forces and moments

The tyre forces and moments from the road surface act on the tyre as shown in Fig. 1. The forces acting along x, y and z axis are longitudinal force F_x, lateral force F_y and normal force F_z, respectively. Similarly the moments acting along x, y and z axis are overturning moment M_x, rolling resistance moment M_y and the self aligning moment M_z, respectively [27].

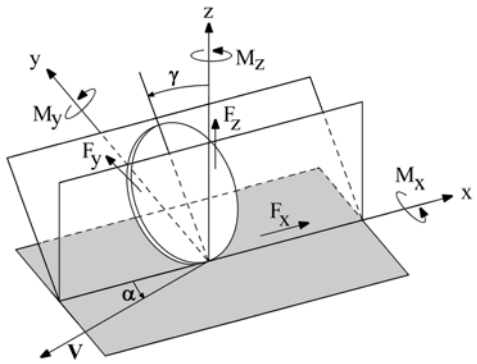

Fig. 1. Tyre forces and moments.

In actual case, the wheel speed and linear acceleration [28] are measured and used to compute the longitudinal slip. The longitudinal slip ratio is defined as the normalized difference between the circumferential velocity and the translational velocity of the wheel [29]. It is expressed as

$$\sigma_x = \begin{cases} \dfrac{\dot{\theta}_{wy} r_w - \dot{x}_w}{\dot{\theta}_{wy} r_w} & \left(\text{during traction, assuming } \dot{\theta}_{wy} \rangle 0\right) \\ \dfrac{\dot{x}_w - \dot{\theta}_{wy} r_w}{\dot{x}_w} & \left(\text{during braking, assuming } \dot{x}_w \rangle 0\right) \end{cases} \tag{1}$$

Lateral wheel slip is the ratio of lateral velocity to the forward velocity of wheel [18]. It is given as

$$\sigma_{\mathrm{y}} = \tan\alpha = \frac{\dot{y}_{\mathrm{w}}}{\dot{x}_{\mathrm{w}}} \tag{2}$$

For small slip ratios, the longitudinal force F_{x} and lateral force F_{y} can be approximated as $F_{\mathrm{x}} = \sigma_{\mathrm{x}} C_{\mathrm{x}}$ and $F_{\mathrm{y}} = \sigma_{\mathrm{y}} C_{\mathrm{y}}$ where, C_{x} and C_{y} are longitudinal tyre stiffness (coefficient) and cornering coefficient, respectively, and σ_{x} and σ_{y} are the longitudinal slip ratio and lateral slip ratio, respectively. However, these linear relations are invalid for large slip ratios.

The empirical magic formula based on experimental data is adopted for the development of tyre-road friction model. It gives more accurate results for larger slip angles. It is also applicable to wide range of operating conditions. Longitudinal slip velocity develops longitudinal force F_{x} whereas side slip velocity and camber angle γ generate side force F_{y} and self aligning moment M_{z}. Pacejka's *magic formula* states that longitudinal force, side force and the self-aligning moment are functions of longitudinal slip and side slip, respectively. It is given as

$$y_{\mathrm{o}} = D\sin\left[C\tan^{-1}\left\{Bx_{\mathrm{i}} - E\left(Bx_{\mathrm{i}} - \tan^{-1}\left(Bx_{\mathrm{i}}\right)\right)\right\}\right] \tag{3}$$

where output variable, $y_{\mathrm{o}} : F_{\mathrm{x}}$, F_{y} or M_{z} and input variable, $x_{\mathrm{i}} : \sigma_{\mathrm{x}}$ or σ_{y}.

Ply-steer, rolling resistance, conicity effects may cause slight variation in the function in Eq. (3), but these variations are may be neglected. The constant parameters $\left(B, C, D, E\right)$ can be determined by measuring the tyre forces and moments by sophisticated equipments.

Pacejka's *magic formula* is unsuitable when snow and ice start significantly affecting the vehicle performance. Moreover, it does not consider the velocity dependence of friction, which is critical while designing brake systems. Therefore, another formula developed by Burckhardt [21] is usually used in research on brake system design. Details of the Burckhardt formulae are given in the next section.

2.2. Antilock braking system

Antilock braking system (ABS) as a vehicle autonomous system can be used to improve stability and to reduce longitudinal stopping distance while maneuvering under braking condition. In [30], it has been shown that antilock braking system approaches the optimum braking performance**.** Antilock braking system is suitable for dangerous braking conditions such as braking on icy or wet asphalt road or for panic braking situation. Upon braking, when the wheel starts slipping, i.e., the slip ratio increases to a maximum desired value, the braking torque is to be reduced

and consequently, the speed of the wheel increases, i.e., the slip ratio decreases. Again when the slip ratio meets a minimum desired value, the braking torque is increased and the process continues [31]. The control of ABS is a combination of slip and wheel acceleration control. In wheel acceleration control, the wheel angular velocities are measured and slip is controlled indirectly by changing the speed of the wheels. Slip cannot be kept at the exact optimum value in a conventional ABS. This is the main drawback for this system. Lots of testing and tuning are required for every ABS controller designed for a specific vehicle. The testing is usually performed through software-in-the-loop and hardware-in-the-loop simulations [32]. Hydraulic valve control is usually used to regulate the brake pressure in antilock braking systems. Kuang *et al.* [33] have modelled hydraulic brake system using the bond graph technique. In [34], sliding mode controllers have been proposed to improve the performance of ABS.

The main components of ABS are brake servo, lever arm, cable, return spring, rod, cam, rotors and brake pads [20]. Schema of an ABS is shown in Fig. 2(a). The ABS controller controls the voltage that is fed to the motor. The resistance is in series with the motor. The lever arm is connected to the motor. The cable is connected to the arm at one end and the other is connected to the lever with cam. The return spring is used to get back to the initial stage.

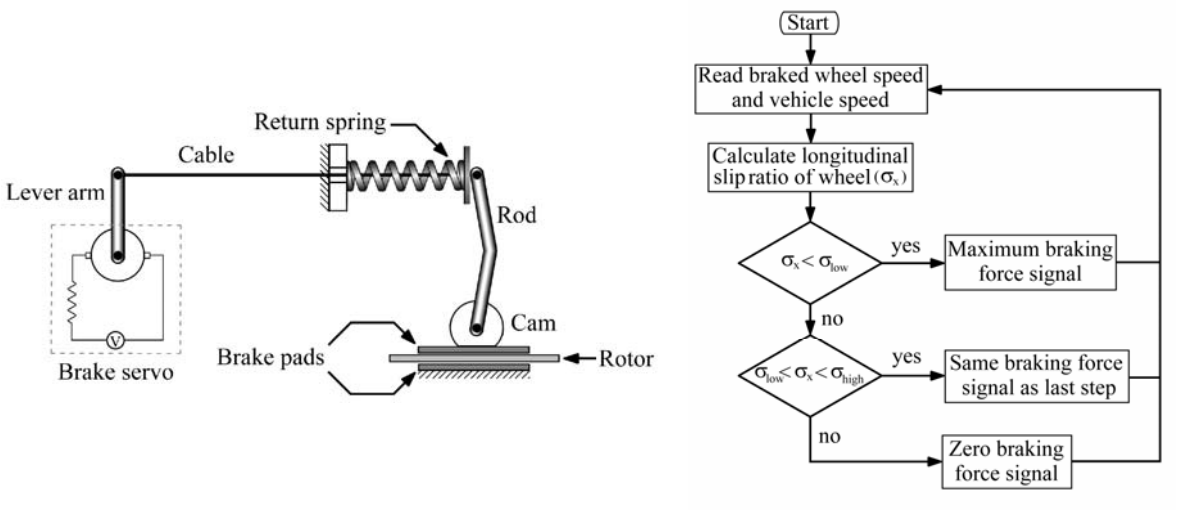

(a) **(b)**

Fig. 2. (a) Schema of an ABS [20] and (b) the flow diagram for ABS algorithm.

The tyre friction models are generally non-linear in nature. The coefficient of friction is

$$\mu = \frac{\sqrt{F_x^2 + F_y^2}}{F_z} \tag{4}$$

where longitudinal force F_x and side force F_y can be determined for particular conditions of constant value of linear and angular velocity from the most widely used *magic formula* (Eq. (3)) given by Pacejka [18] and F_z is the normal force. However, one main disadvantage of this model is its inability to describe low slip effects and large forward and side slip effects during wheel lockup.

Another friction model often used to model tyre forces is given by Burckhardt as follows [21]

$$\mu(\sigma_x, \dot{x}_w) = \left[C_1 \left(1 - e^{-C_2 \sigma_x}\right) - C_3 \sigma_x \right] e^{-C_4 \sigma_x \dot{x}_w} \tag{5}$$

where constant parameters C_1, C_2, C_3 and C_4 are determined from experiments. These parameters for various road conditions [21] are given in Table 1. The slip-friction curve obtained from this model is shown in Fig. 4.

The flow chart for the ABS algorithm used in this article is shown in Fig. 2(b). Here the longitudinal slip is switched between maximum and minimum values and, accordingly, brake force signal changes and ultimately the braking torque varies as follows:

$$\tau_i = \begin{cases} \tau_{max} & \sigma_x < \sigma_{low} \\ \tau_{i-1} & \sigma_{low} \le \sigma_x \le \sigma_{high} \\ 0 & \sigma_x > \sigma_{high} \end{cases} \tag{6}$$

Table 1. Tyre-road friction parameters [21]

Surface condition	C_1	C_2	C_3	C_4
Asphalt, dry	1.029	17.16	0.523	0.03
Asphalt, wet	0.857	33.822	0.347	0.03
Cobblestones, dry	1.3713	6.4565	0.6691	0.03
Snow	0.1946	94.129	0.0646	0.03

The slip–friction curve for a wheel traveling with linear speed of 10 m/s for various road conditions is shown in Fig. 3. It is seen from this figure that the coefficient of friction increases with the increase of slip to a maximum value and then it decreases monotonically. If the wheel gets locked $(\sigma_x = 1)$ then value of the coefficient of friction is low and the wheel starts sliding and the steering control may be lost, which is totally undesirable. To increase steerability and lateral stability of the vehicle and to decrease the stopping distance during braking, the slip value must be maintained within a range to get the high value of friction force. As the slip dynamics is very fast and at any value after the peak of the friction curve is open loop unstable, the slip value is kept within a

certain range which is also called *sweet–spot* (see the shaded area in Fig. 3). The attainable maximum friction coefficient is different at different vehicle speeds (See Fig. 4). Brake systems are designed to give maximum braking efficiency at higher speeds. Moreover, it is usually impossible to reliability ascertain the road condition from onboard measurements. In ABS design, the optimal slip ratio range is thus taken to be 0.2–0.25. This range offers a good compromise where near maximum friction coefficient is achieved for all kinds of road surfaces (thus, eliminating the requirement of road condition recognition) and vehicle linear speed.

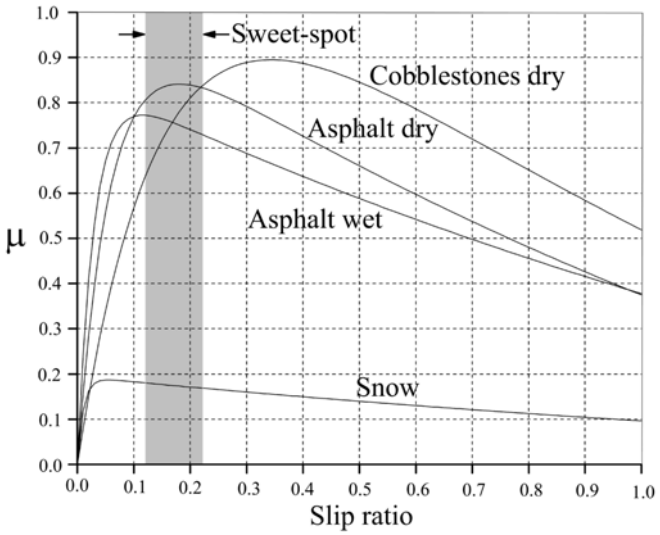

Fig. 3. Friction coefficient versus slip ratio curves for different road surfaces at linear speed of 10m/s with the tire properties given in [21].

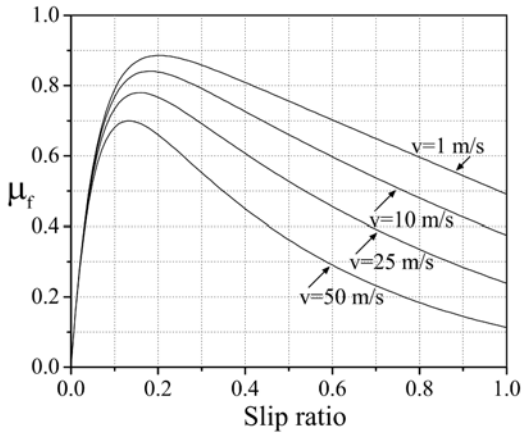

Fig. 4. Slip-friction curves for asphalt dry road condition for different vehicle speeds.

3. Bicycle vehicle model

A bicycle model of the vehicle [35] was used for the initial study. This model does not take into account the roll, pitch and heave motions and the suspension dynamics is neglected. Thus, the load transfer during maneuvering and

braking cannot be included in this model. Schematic of the considered vehicle is shown in Fig. 5(a) and its word bond graph is shown in Fig. 5(b). As the road is considered to be flat, the motion of the vehicle is planar.

3.1. Kinematic relations

The kinematic relations derived in [2, 35] are used to construct a major part of the model. Thereafter, the wheel rotations and longitudinal and lateral slip calculations are inserted into the model. It is assumed that only the front wheel is steered (by steering angle δ).

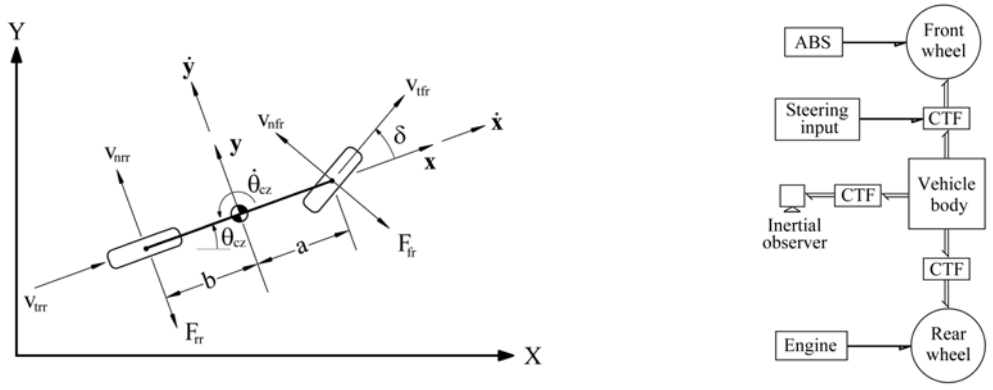

(a) **(b)**

Fig. 5. (a) Schema of the bicycle vehicle model; and its (b) Word bond graph.

Velocities normal and tangential to the plane of rotation of the front wheel are

$$\begin{aligned} v_{\text{nfr}} &= (\dot{y} + \dot{\theta}_{\text{cz}} a)\cos\delta - \dot{x}\sin\delta \\ v_{\text{tfr}} &= (\dot{y} + \dot{\theta}_{\text{cz}} a)\sin\delta + \dot{x}\cos\delta \end{aligned} \tag{7}$$

Likewise, velocities normal and tangential to the plane of rotation of the rear wheel are

$$v_{\text{nrr}} = (\dot{y} - \dot{\theta}_{\text{cz}} b), v_{\text{trr}} = \dot{x} \tag{8}$$

From Newton-Euler equations with $z = \dot{\theta}_{cx} = \dot{\theta}_{cy} = 0$, one obtains

$$\begin{aligned} m_{\text{v}}\ddot{x} &= m_{\text{v}}\,\dot{\theta}_{\text{cz}}\,\dot{y} + \sum F_x \\ m_{\text{v}}\ddot{y} &= -m_{\text{v}}\,\dot{\theta}_{\text{cz}}\,\dot{x} + \sum F_y \end{aligned} \tag{9}$$

3.2. Bond graph model

In the word bond graph of the bicycle vehicle model shown in Fig. 5(b), CTF blocks represent necessary coordinate transformations [36]. Maintaining the model structure defined in the word bond graph, the complete bond graph model as shown in Fig. 6 can be drawn using Eqs. (7–9). The terms $m_{\text{v}}\,\dot{\theta}_{\text{cz}}\,\dot{y}$ and $-m_{\text{v}}\,\dot{\theta}_{\text{cz}}\,\dot{x}$ in Eq.(9) are conservative pseudo-forces which are implemented by a gyrator (GY) element in the bond graph model. In Fig. 6, lines with half-arrow at their end are power bonds and those with a full arrow at their end are information bonds.

The vehicle inertias ($\mathrm{I}:m_v$) are modeled in the moving frame and the pseudo-forces transform them to inertial frame. The rotary inertia ($\mathrm{I}:J_v$) is modeled at a 1-junction. The transformer elements (TF) are used to calculate the tangential and normal velocities at tyres according to Eqs. (7–8). The flow detectors (Df) connected to velocity points in the inertial frame are not present in the actual system, *i.e.*, the actual system is not instrumented with an inertial sensor. These flow detectors are simply added to plot the x and y positions of the vehicle centre of mass in the inertial frame and also to modulate the modulated transformer elements in the part of the junction structure.

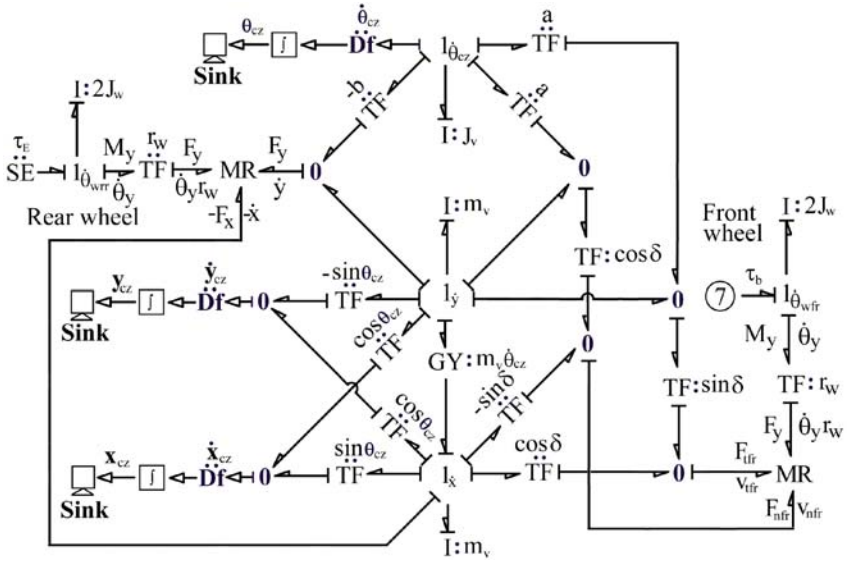

Fig. 6. Bond graph model of bicycle vehicle model.

Port number 7 shown within a circle is used to interface this model to the model of the brake system. The two modulated 3-port R-fields (MR-elements) implement Pacejka's magic formulae. First of all, the velocity of the contact patch on the tyre, the longitudinal velocity of the tyre and the lateral velocity are used to compute the longitudinal and lateral slip ratios according to Eqs. (1–2). Thereafter, Eq. (5) is used to compute the coefficient of friction and the net frictional force. The components of the net frictional force are used to compute the longitudinal and lateral tyre forces and the reaction moment on the drive. The self-aligning moment is not included in the bicycle model. Thus, the MR-element, as causalled in the model, receives the information of three generalized flow variables and computes three generalized effort variables.

3.3. Braking system

A comparison between the bond graph model of mechanical equivalent braking system (Fig. 2(a)) and the conventional hydraulic braking system is shown in Fig. 7. In hydraulic braking system, the pedal force F_{pedal} is

represented by the Se element (Fig. 7(b)). The fluid flow through supply or hold valve is modelled by a resistive element R_{sv}. The element C connected with 0 junction, which determines pressure of brake cylinder, indicates the brake fluid compressibility K_{β} (a function of bulk modulus and fluid volume). R_{rv} is the resistance in the pressure relief valve and atmospheric pressure is indicated by the zero-valued Se element. Braking torque depends on the area of the brake cylinder and the radius of the brake drum.

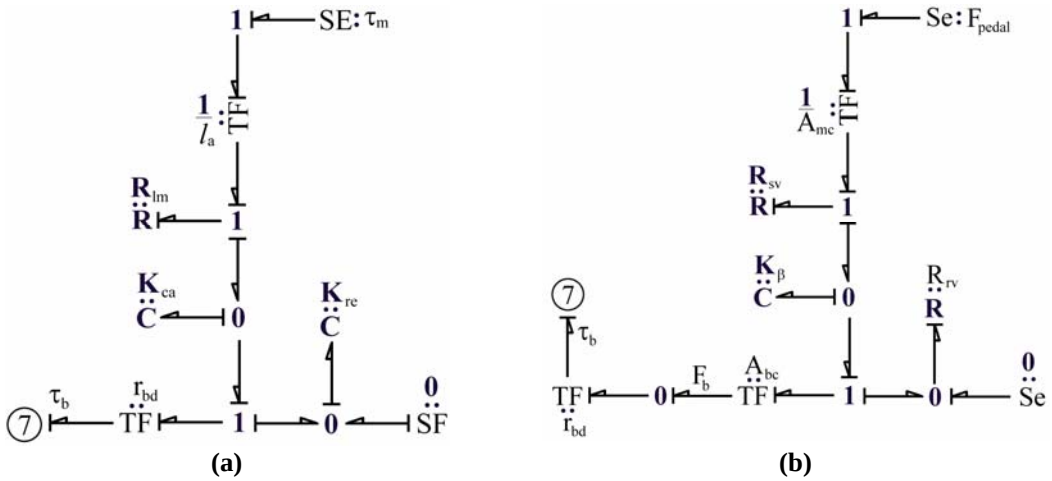

Fig. 7. Bond graph model of (a) Mechanical equivalent braking system; and (b) Hydraulic braking system

In the bond graph model of the mechanical equivalent braking system [20] shown in Fig. 2(a), the controlled voltage from the ABS controller is fed to the motor whose generated torque (τ_m) is represented by a Se element. The resistive element connected to 1 junction denotes mechanical losses (R_{lm}). The cable stiffness is represented by C element connected to 0-junction. The return spring having stiffness K_{re} is represented by C element. The other end of the return spring is anchored to the ground by a zero-valued source of flow. The output braking torque is applied on the bicycle vehicle model (Fig. 6) and wheel model for full vehicle through port 7.

3.4. Model validation

The model parameters used in the simulation of the bicycle vehicle model are given in Table 2. Implementations of ABS on the planar bicycle model are first carried out to fine-tune and test the control algorithm. Once the controller implementation (program) was found to be satisfactory, it was ported to the full vehicle model.

The validation of the ABS system has been performed by comparing the results with those reported in [20]. Considering the fact that steering effect was not considered in [20], the steering angle in the bicycle model was kept zero. The vehicle weight and the initial linear and angular velocities of the wheels are taken to be the same as those

in [20] and the rear wheel of the vehicle is considered to be freely rolling. With these adjustments to match the scenarios, the ABS bicycle model developed here is nearly equivalent to that presented in [20].

Table 2. Parameter values of bicycle vehicle model.

Subsystem	Parameter values			
Vehicle body	$m_v = 1600$ kg	$J_v = 100$ kg m^2	$a = 1.0$ m	$b = 1.0$ m
Wheel	$J_w = 15$ kg m^2	$r_w = 0.3$ m		
	$C_1 = 1.029$	$C_2 = 17.16$	$C_3 = 0.523$	$C_4 = 0.03$
Antilock brake	$\sigma_{low} = 0.04$	$\sigma_{high} = 0.5$	$K_{ca} = 10^4$ N/m	$K_{re} = 10^6$ N/m
	$r_{bd} = 0.15$ m	$R_{lm} = 0.04$ N s/m	$l_a = 1$ m	$\mu_m = 0.4$ N m/A
	$R_{aero} = 0.1$ kg/s			

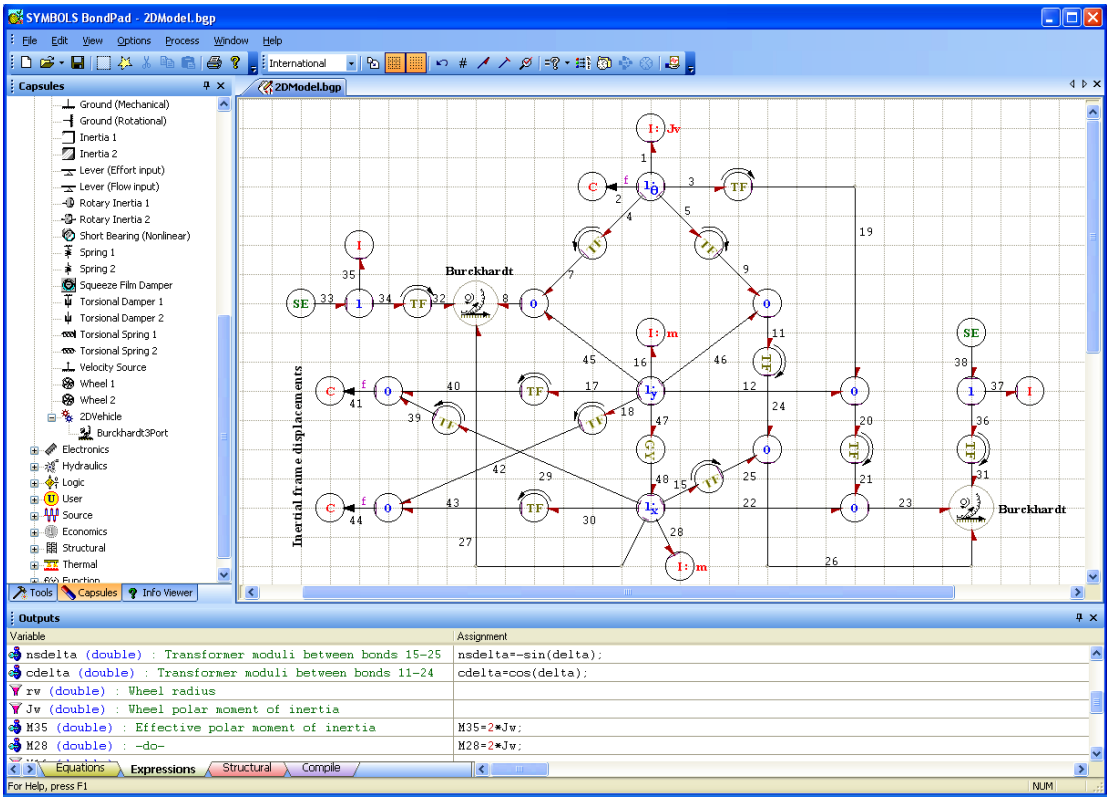

Fig. 8. Modelling environment in Symbols software: the left panel contains bond graph elements and subsystem models called capsules, the bottom panel displays equations derived from bond graph model in the equations tab and the user can enter model parameter descriptions, model nonlinearity expressions *etc.* in the expressions tab.

All simulations presented in this article are performed in Symbols software [37] which is an integrated platform for port-based modeling using bond graphs and block diagrams, simulation, animation, control system analysis and fault detection and isolation system design [38, 39]. The software runs in Windows and Linux operating systems. It follows an object oriented modeling framework in which subsystem models can be

developed, validated and integrated [40]. One of the major advantages of Symbols software is its implementation of polymorphic objects which allows template matching for varying boundary causalities. The modeling environment is shown in Fig. 8 where the bond graph model of the bicycle vehicle has been displayed. The C-elements with signal bonds in Fig. 8 together represent the detector of flow (Df) elements and sinks. The MR elements in Fig. 6 are modeled as a subsystem (represented by its icon) in Fig. 8. This user created subsystem appears in the list of subsystem objects called capsules. The software has many in-built capsules for basic engineering components.

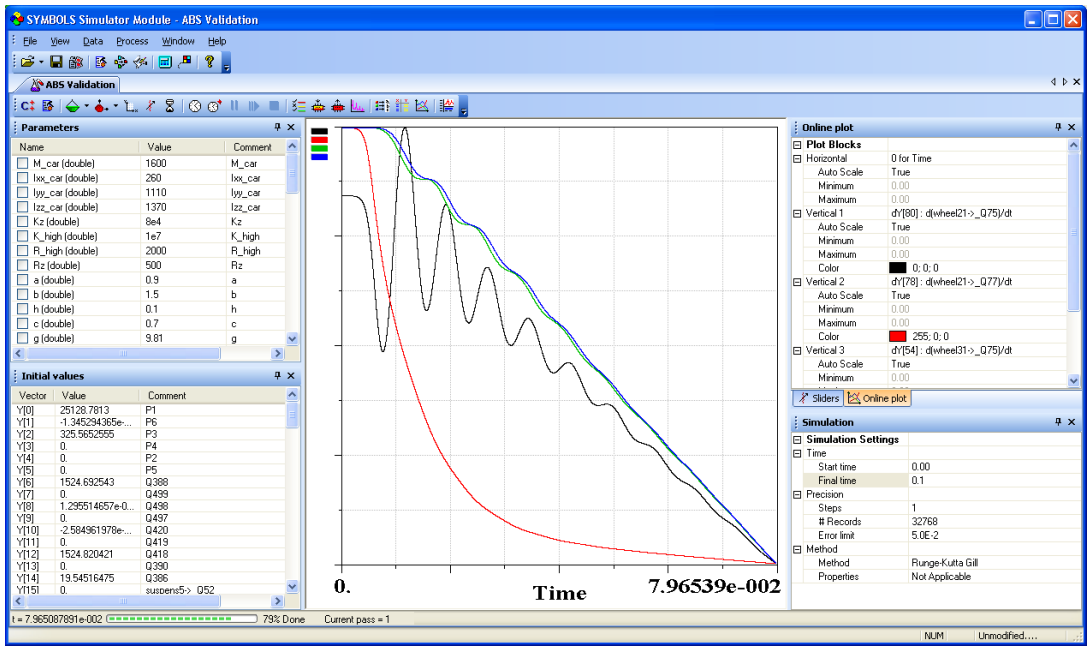

Fig. 9. The simulation environment in Symbols software contains tabs for parameter, initial condition, plot variables and simulation setting entries. The slider tab is for runtime parameter variation by the user. The runtime display is not scaled properly and a separate graphics display window appears after the end of simulation.

The equations of motion are derived by Symbols software from the bond graph model. These equations can be exported in various ways such as in S-function form for Matlab simulink, C++ source code for user written solvers, *etc.* Symbols software also has a powerful native solver (See Fig. 9) which offers a vast range of simulation and post processing tools.

The simulation of ABS system is a combination of continuous time and discrete time simulation. The measurements are acquired from the model at intervals of 0.2ms (sampling frequency of 5kHz) and a zero-order-hold is used with each measurement. The simulation time step is chosen to be 0.1ms. The same simulation setting is used for all results presented in this article.

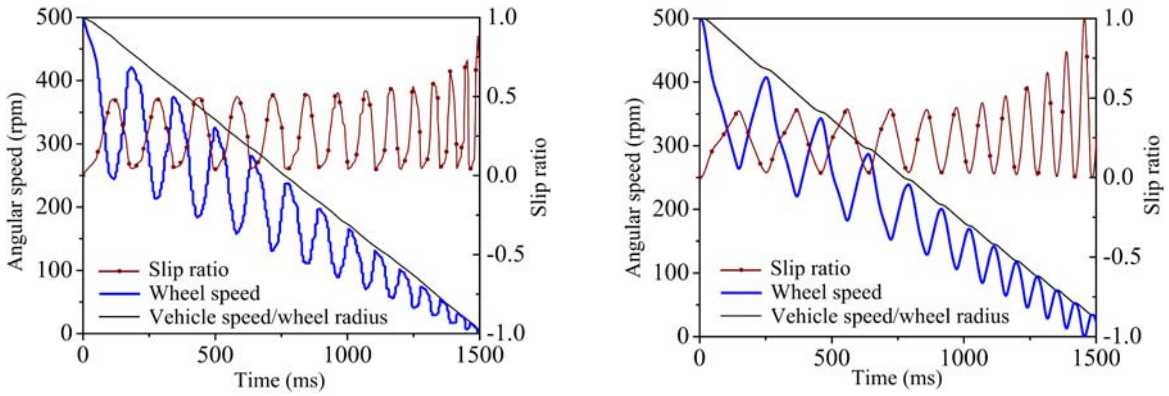

Fig. 10. Vehicle speed, wheel speed and wheel slip ratio (a) as reported in [20] and (b) as obtained from the bicycle model during full braking by ABS.

Figure 10 shows a comparison of the results reported in [20] with those obtained from the developed ABS bicycle model. Both the results show almost linear variations in the forward linear wheel speed and a regular pattern of deceleration and acceleration of the wheel angular speed. The slip ratios are initially maintained within a bound and as the vehicle slows down, their maximum values approach unity. The variations in the results are mainly due to the differences in the considered dynamics. The four wheel model of [20] is influenced by vehicle's pitch during braking and thus the load transfer to the front wheels (where ABS brakes are applied) produces marginally higher braking force than the bicycle model. Therefore, the results in Fig. 10(a) show slightly fast braking action as compared to those in Fig. 108(b).

3.5. ABS performance while braking during maneuvering

The ABS is meant to provide better maneuverability while brakes are applied on the steered wheel. To evaluate the maneuverability of the vehicle under braking situation, a particular scenario has been considered here. First of all, the vehicle starts from rest and it is brought to a steady linear speed of 50 km/h over a straight path. Then it is steered at $t = 12$ s to follow a circular path with a constant steering angle of 0.1 radians. The steering action causes a decrease in the vehicle linear speed. Once the vehicle linear speed is stabilized and it moves at constant speed over the circular path, front wheel brakes are applied at $t = 17$ s. Note that to handle large side and forward slips during wheel lockup, a composite slip based formulation [41] developed by U.S department of transportation (DOT) has been adopted.

Figure 11(a) shows the predefined path (2.5m wide lane) over which the vehicle is supposed to move and the actual paths taken by the vehicle under two different braking conditions: the first when ABS is used and the second when a conventional mechanical brake is used. In the ABS, slip control strategy to keep the slip ratios

between 0.2–0.25 is applied. Initially, a sustained brake force is applied till the slip ratio becomes 0.2 and then the slip control algorithm takes over. The result shows that the vehicle veers off from the lane due to application of the conventional brake whereas it stays within the lane till it stops when ABS is used.

The results in Fig. 11(b) show the change in slip ratios due to braking. The slip ratios for ABS remain within 0.2 to 0.25 and thus the vehicle is able to follow the steering. The slip ratio quickly approaches a value of 1.0 due to application of conventional brake. This causes the wheels to lock up and thus the vehicle cannot steer.

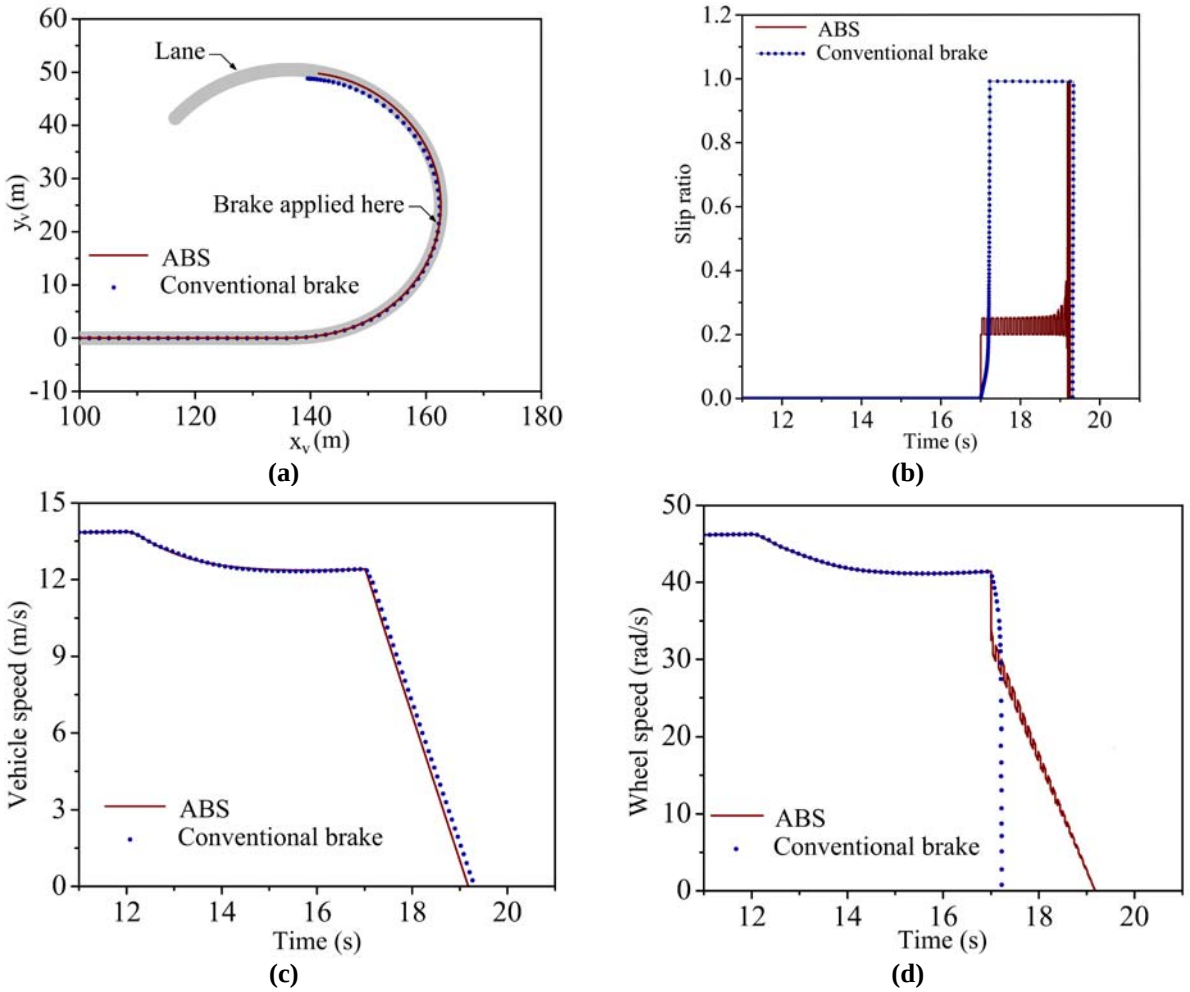

Fig. 11. (a) Vehicle centre of mass trajectory in inertial frame; (b) Wheel slip ratio; (c) Vehicle speed; and (d) Wheel speed for ABS and conventional braking system.

Figure 11(c) shows the vehicle speed variations due to steering and braking and Fig. 11(d) shows the angular velocity of the front wheel under the same condition. The wheel locks up due to application of conventional brake as soon as the wheel speed becomes zero. However, on application of ABS there is an initial sudden drop in wheel speed (till the slip ratio becomes 0.2) and then the wheel speed decelerates and accelerates much like the results shown in Fig. 10(b). The linear speed of the vehicle reduces almost linearly to zero in both case; the

deceleration (See Fig. 11(c)) being slightly faster for ABS as compared to the conventional brake. This deceleration almost doubles when brakes are applied both on the front and the rear wheels. With the ABS based on slip control mechanism, the vehicle stops faster and at a shorter distance. The results suggest that an automatic lane departure monitoring and control system [42] should also involve the brake system (standard, ABS, ...) in the control loop.

4. The bond graph for the four wheel model

The four wheel vehicle system is modeled by composing six subsystem models. These are: vehicle body, suspension, wheel, steering, antilock braking system and differential. The word bond graph representation of the full vehicle model is shown in Fig. 12 where bonds represented by two parallel lines are multi-bonds. The flow variables at the interface of different subsystems are marked in Fig. 12. The complimentary power variables or generalized effort variables (force for linear velocity and torque for angular velocity) are not shown in Fig. 12 to maintain clarity of the figure. The four wheels are connected with the vehicle body through suspensions. The steering and ABS are coupled with the axle by scalar bonds. Likewise, scalar bonds connect the differential to the rear wheels and the vehicle body. The engine and the gear box are disengaged during braking, so they are not shown here although they are included in the full model. The integrated model may be reduced further for specific operational conditions [36].

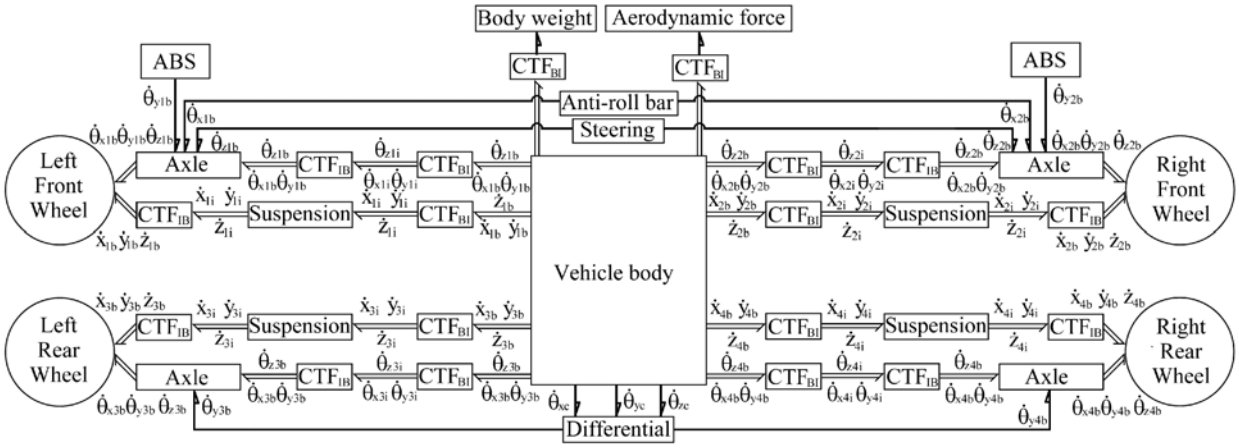

Fig. 12. Word bond graph of four wheel vehicle model.

4.1. Vehicle body

The full vehicle schema is shown in Fig. 13. It is assumed that the vehicle is symmetrical with respect to its longitudinal axis. The suspension is approximated by simple linear spring-damper suspension system which corresponds to energy storage and energy dissipation at each corner of the vehicle body while allowing free rotation of the wheel about axle (y-axis). The vehicle body motion is described by three linear displacements along three body-fixed axes and the rotational motion of the body is defined by the three Cardan angles. The Newton–Euler

equations with attached body fixed axes aligned with the principal axes of inertia are as used for modeling the vehicle body [24].

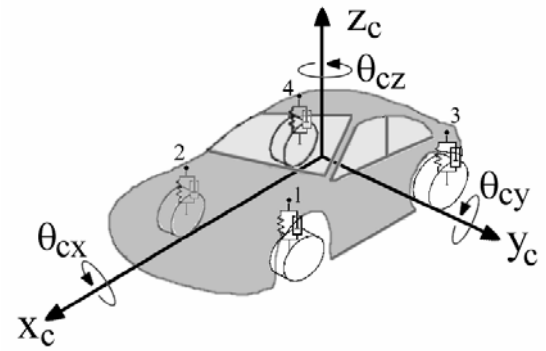

Fig. 13. Four-wheel vehicle model.

The vehicle body is modeled as a rigid body with six degrees of freedom, i.e., pitch, roll, yaw, heave, surge, and sway motions. The rigid body motion is described with respect to a coordinate system rotating and translating with it. This local coordinate frame attached at the centre of mass of the body is assumed to be aligned with the inertial principal axes. The motion of the vehicle body is described by three linear displacements along body-fixed x, y and z axes (See Fig. 13) and rotations about those axes. The vehicle orientation is defined by the three Cardan angles. The Newton-Euler equations of the vehicle body [24] with attached body fixed axes aligned with the principal axes of inertia are as follows:

$$\sum F_{\mathrm{x}} = m_{\mathrm{c}}\ddot{x}_{\mathrm{c}} + m_{\mathrm{c}}(\dot{z}_{\mathrm{c}}\dot{\theta}_{\mathrm{cy}} - \dot{y}_{\mathrm{c}}\dot{\theta}_{\mathrm{cz}}) \tag{10}$$

$$\sum F_{\mathrm{y}} = m_{\mathrm{c}}\ddot{y}_{\mathrm{cb}} + m_{\mathrm{c}}(\dot{x}_{\mathrm{c}}\dot{\theta}_{\mathrm{cz}} - \dot{z}_{\mathrm{c}}\dot{\theta}_{\mathrm{cx}}) \tag{11}$$

$$\sum F_{\mathrm{z}} = m_{\mathrm{c}}\ddot{z}_{\mathrm{c}} + m_{\mathrm{c}}(\dot{y}_{\mathrm{c}}\dot{\theta}_{\mathrm{cx}} - \dot{x}_{\mathrm{c}}\dot{\theta}_{\mathrm{cy}}) \tag{12}$$

$$\sum M_{\mathrm{x}} = J_{\mathrm{cx}}\ddot{\theta}_{\mathrm{cx}} - \dot{\theta}_{\mathrm{cy}}\dot{\theta}_{\mathrm{cz}}(J_{\mathrm{cy}} - J_{\mathrm{cz}}) \tag{13}$$

$$\sum M_{\mathrm{y}} = J_{\mathrm{cy}}\ddot{\theta}_{\mathrm{cy}} - \dot{\theta}_{\mathrm{cz}}\dot{\theta}_{\mathrm{cx}}(J_{\mathrm{cz}} - J_{\mathrm{cx}}) \tag{14}$$

$$\sum M_{\mathrm{z}} = J_{\mathrm{cz}}\ddot{\theta}_{\mathrm{cz}} - \dot{\theta}_{\mathrm{cx}}\dot{\theta}_{\mathrm{cy}}(J_{\mathrm{cx}} - J_{\mathrm{cy}}) \tag{15}$$

The first three equations (Eqs. (10–12)) are Newton's equations where pseudo-forces appear due to the use of body-fixed or non-inertial frame. The later three equations (Eqs. (13–15)) are Euler's equations which account for gyroscopic moments. Note that the linear and angular velocities used in Newton-Euler equations are velocities as

seen from a frame that is momentarily aligned with the body-fixed principal axes. The whole set of six equations is referred to as Newton-Euler equations. Euler's equations are represented in a bond graph form called Euler Junction Structure (EJS) [1–3, 5, 24].

Consider a rigid body of mass *m*, moments of inertia about principal axes (x,y and z) with origin at the mass centre as I_{xx}, I_{yy} and I_{zz}, angular velocities as seen from an inertial frame momentarily aligned along body fixed principal axes as ω_x, ω_y and ω_z, external moment components as M_x, M_y and M_z, external force components as F_x, F_y and F_z. The general form of EJS for the rigid body is shown in Fig. 14(a). Another such gyrator ring structure is used to model the Newton's equations. The Newton-Euler equations are represented in bond graph form by combining both to form a star-shaped junction structure given in Fig. 14(b).

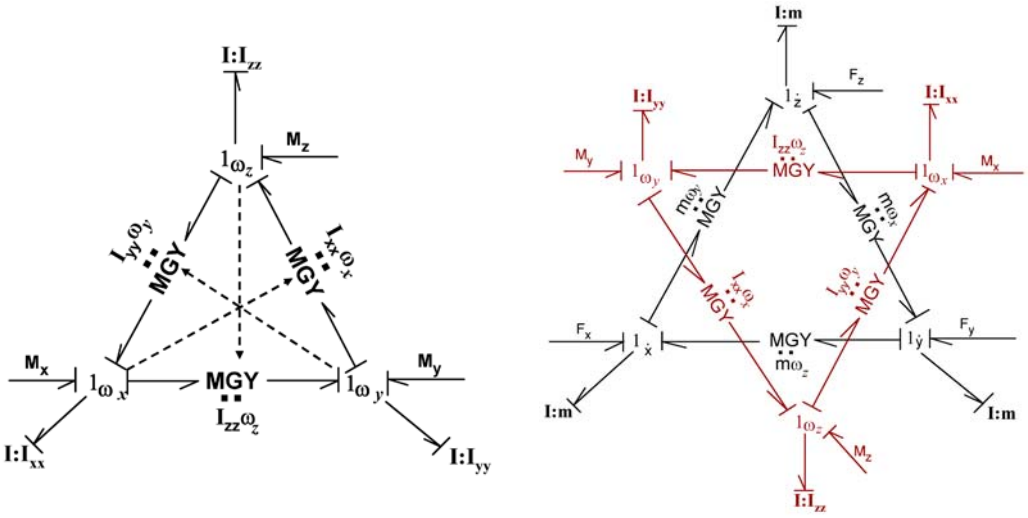

Fig. 14. Bond graph model of (a) Euler junction structure and (b) Newton-Euler equations

Figure 14(b) is the basic building block to construct the bond graph model of a multibody system. The next modelling step involves computation of velocities of certain points on the rigid body, transformation of those into inertial frame velocities and implementation of the physical constraints at the chosen points. Note that in a bond graph model, implementation of kinematic constraints at a set of points also accounts for the dynamic constraints, *i.e.*, the external forces and moments resulting from those constraints. This happens due to the power conserving junction structure. Therefore, bond graph modelling is very useful in developing complex system models.

The equations for three linear velocities of left–front suspension reference point (point 1 in Fig. 13 whose body fixed coordinates are x_1, y_1, z_1) in the moving system of axes are as follows:

$$\dot{x}_1 = \dot{x}_c + z_1\dot{\theta}_{cy} - y_1\dot{\theta}_{cz} \tag{16}$$

$$\dot{y}_1 = \dot{y}_c + x_1\dot{\theta}_{cz} - z_1\dot{\theta}_{cx} \tag{17}$$

$$\dot{z}_1 = \dot{z}_c + y_1\dot{\theta}_{cx} - x_1\dot{\theta}_{cy} \tag{18}$$

The equations for the three angular velocities of left front suspension reference point are similarly expressed. Likewise, the equations for three linear velocities and three angular velocities of other suspension reference points are derived.

The velocity transformation from the moving frame to the inertial frame can be written using successive multiplication of rotation matrices as follows:

$$\begin{Bmatrix} \dot{X} \\ \dot{Y} \\ \dot{Z} \end{Bmatrix} = \mathbf{T}_{\psi,\theta,\varphi} \begin{Bmatrix} \dot{x} \\ \dot{y} \\ \dot{z} \end{Bmatrix} \text{ and } \begin{Bmatrix} \omega_X \\ \omega_Y \\ \omega_Z \end{Bmatrix} = \mathbf{T}_{\psi,\theta,\varphi} \begin{Bmatrix} \omega_x \\ \omega_y \\ \omega_z \end{Bmatrix}, \tag{19}$$

where

$$\mathbf{T}_{\psi,\theta,\varphi} = \underbrace{\begin{bmatrix} \cos\psi & -\sin\psi & 0 \\ \sin\psi & \cos\psi & 0 \\ 0 & 0 & 1 \end{bmatrix}}_{\mathbf{T}_\psi} \underbrace{\begin{bmatrix} \cos\theta & 0 & \sin\theta \\ 0 & 1 & 0 \\ -\sin\theta & 0 & \cos\theta \end{bmatrix}}_{\mathbf{T}_\theta} \underbrace{\begin{bmatrix} 1 & 0 & 0 \\ 0 & \cos\phi & -\sin\phi \\ 0 & \sin\phi & \cos\phi \end{bmatrix}}_{\mathbf{T}_\varphi} \tag{20}$$

and ψ, θ and ϕ are the Z-Y-X Cardan angles (a form of Euler angles). This power conserving Coordinate Transformation can be represented by a bond graph junction structure (CTF or coordinate transformation block) [36]. Inverse transformation of velocities in inertial frame to body-fixed frame can be represented by a similar junction structure [36].

The angles used in Eq. (20) are the Cardan angles (Euler angles). Transformation from body-fixed angular velocities to Euler angle rates is given by

$$\begin{Bmatrix} \dot{\phi} \\ \dot{\theta} \\ \dot{\psi} \end{Bmatrix} = \begin{bmatrix} 1 & 0 & -\sin\theta \\ 0 & \cos\phi & \cos\theta\sin\phi \\ 0 & -\sin\phi & \cos\theta\cos\phi \end{bmatrix}^{-1} \begin{Bmatrix} \omega_x \\ \omega_y \\ \omega_z \end{Bmatrix} = \begin{bmatrix} 1 & \tan\theta\sin\phi & \tan\theta\cos\phi \\ 0 & \cos\phi & -\sin\phi \\ 0 & \sin\phi/\cos\theta & \cos\phi/\cos\theta \end{bmatrix} \begin{Bmatrix} \omega_x \\ \omega_y \\ \omega_z \end{Bmatrix}. \tag{21}$$

The transformations given in Eq. (21) are represented in bond graph form as a transformer junction structure (EATF or Euler angle transformation block). The Euler angle rates are integrated to obtain the Euler

angles, which are used in all coordinate transformations, *i.e.*, in CTF and EATF bond graph sub-models. Note that for the vehicle body, $\omega_x = \dot{\theta}_{cx}, \omega_y = \dot{\theta}_{cy}, \omega_z = \dot{\theta}_{cz}$, $I_{xx} = J_{cx}, I_{yy} = J_{cy}$ and $I_{zz} = J_{cz}$. For the geometric parameters defined in the nomenclatures, the suspension reference point 1 coordinates are $x_1 = a$, $y_1 = c$ and $z_1 = -h$. The other reference point coordinates are similarly expressed and used in kinematic relations.

The bond graph in Fig. 15 models the vehicle body inertia and transformations of the three linear and three angular velocities into velocities at relevant suspension reference points. The inertias are coupled by a pair of gyrator rings (Euler junction structure [1, 2, 13, 16]), one for translational and the other for rotational velocities.

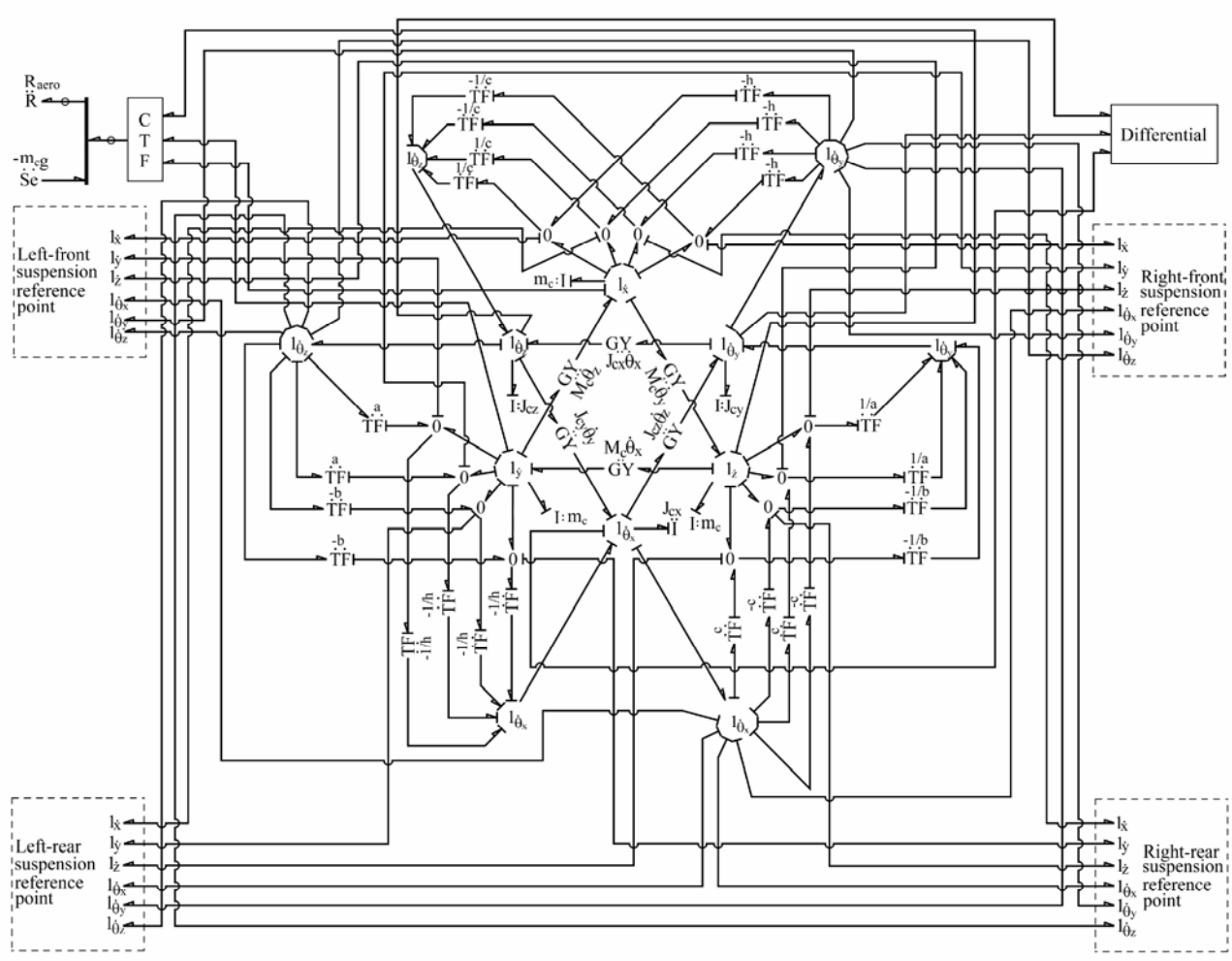

Fig. 15. Bond graph model of vehicle body.

Three sets of forces and moments act on the body. First of all, weight of the body and the aerodynamic forces (modeled by R_{aero} element) in the inertial frame act the vehicle body model in non-inertial frame through

coordinate transformation (CTF). Secondly, engine torque which is in a different body fixed frame (wheel frame) is transformed twice (first from wheel body fixed frame to inertial frame and then to vehicle body fixed frame) to act on the body. Lastly, the suspension forces and moments (constraint forces) acting in the inertial frame are transformed to get forces in the body fixed direction. Then these forces are multiplied with the moment arms. The forces at all the four corners of the body are added together to get the suspension force acting at the centre of gravity of the body.

4.2. Wheels

The bond graph model of wheel is shown in Fig. 16. The wheel is modeled as a rigid body with six degrees of freedom. Similar to vehicle body, the inertias are coupled by a pair of gyrator rings, one for the translational and the other for the rotational velocities.

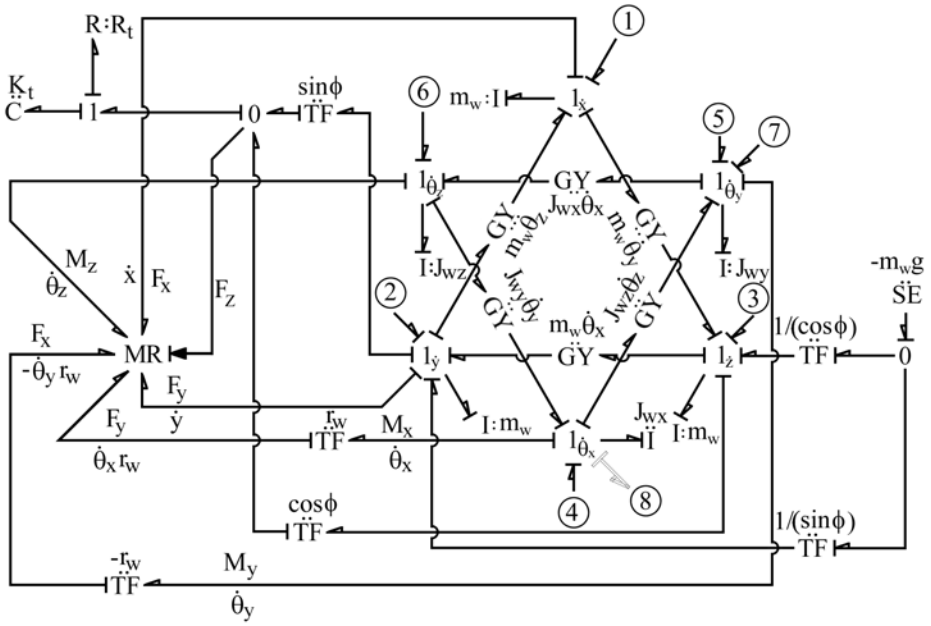

Fig. 16. Bond graph model of a wheel.

There are some basic differences between the vehicle body model and the tyre model. The suspension reference points in the vehicle body are fixed points. On the other hand, the tyre-road contact point in the wheel is not a point fixed on the wheel; it changes as the wheel rotates about the axle. The second difference is that the wheel rotation about its axle axis does not change its orientation in the inertia frame. Here, the wheel and its axle are assumed to be rotationally symmetric about an axis.

The tyre-road normal contact force and the gravity force always act along inertial Z-axis. Thus, the wheel vertical dynamics is decoupled from longitudinal and cornering dynamics. The ground reaction force (F_Z) and wheel radius (r_w) are used to modulate longitudinal and cornering dynamics which are given in axle body-fixed frame. The vertical velocity of the wheel is computed through a set of transformations at a 0-junction which is connected to a 1-junction where the vertical stiffness and damping of tyre (represented by K_t and R_t , respectively) are modelled. The angle ϕ used in the transformations (to obtain wheel vertical motion at contact patch and to model self weight of the wheel and axle) is the wheel tilt with respect to the ground, *i.e.* the angle of rotation of the wheel about X-axis of an momentarily conceived inertial frame whose Z-axis is along inertial vertical direction and y-axis is aligned along the axle. The title angle may include additional camber. The coordinate transformations are performed through the transformer structures shown in the model, *i.e.*, a separate CTF block is not required here.

The MR-element which is used for modelling road-tyre interactions is modulated by the normal reaction in the inertial frame. Kinetic phenomenon and weight of the wheel are considered for the un-sprung mass vertical dynamics. The tyre-road interactions and braking action are considered for wheel longitudinal and cornering dynamics. The cornering force and self-aligning moment are dependent on vertical load and lateral slip angle, while the longitudinal force is dependent on vertical load and longitudinal slip rate. The characteristic relations for the MR-element are given according to Burckhardt's formulae [21] or the composite slip based formulation [41].

Ports 1–6 in Fig. 16 are connected to the corresponding velocities of the suspension reference points. The braking torque is applied on the front wheel through port 7 and the engine torque is transmitted to the rear wheel through the port 7. Port 8 is (shown as by dotted bond) is present only for front wheels. This port is used to interface the front wheel model to the anti-roll bar model, which constrains the relative roll between two front wheel axles. The steering torque is applied at port 4 through the steering column model given in Fig. 17.

4.3. Steering system

In this article, we are directly modeling the input from the human operator. The moment applied on steering wheel about the z-axis is supplied as shown in Fig. 17(a). The actual the rate of rotation of steering wheel is measured by a yaw rate sensor. It is assumed that the human vision system prescribes the desired rate of rotation. A feedback yaw

rate controller may be developed where the controller action can mimic the driver's response to the consequences of steering. The steering model output is used to rotate the front wheels by applying torques on the front axle (and reactive torques on the vehicle body). The rotary inertia J_{st} of the steering wheel is represented by I-element. The remainder of the system comprises mechanical transmission to the front axle. The rate of rotations of left and right wheels about the z-axis are represented at $1_{\dot{\theta}_l}$ and $1_{\dot{\theta}_r}$ junctions. These are interfaced to the front axle model through ports 9 and 10. The modulated transformer moduli m_1 and m_2 are determined from Ackermann's formulae given as

$$\dot{\delta}_i = \left[\frac{(a+b)\cos^2\theta_l + c\tan\theta_l\cos^2\theta_l}{(a+b)\cos^2\theta_{st} - c\tan\theta_{st}\cos^2\theta_{st}}\right]\dot{\delta} \tag{16}$$

$$\dot{\delta}_o = \left[\frac{(a+b)\cos^2\theta_r - c\tan\theta_r\cos^2\theta_r}{(a+b)\cos^2\theta_{st} + c\tan\theta_{st}\cos^2\theta_{st}}\right]\dot{\delta} \tag{17}$$

In experimental investigations, steering wheel rotations (driver inputs) are measured. The model in Fig. 17(a) may be modified to the form shown in Fig. 17(b) to take the rate of steering wheel rotation as the input. The transformer with modulus μ_{stw} is the gear ratio between steering wheel rotation and steering rotation.

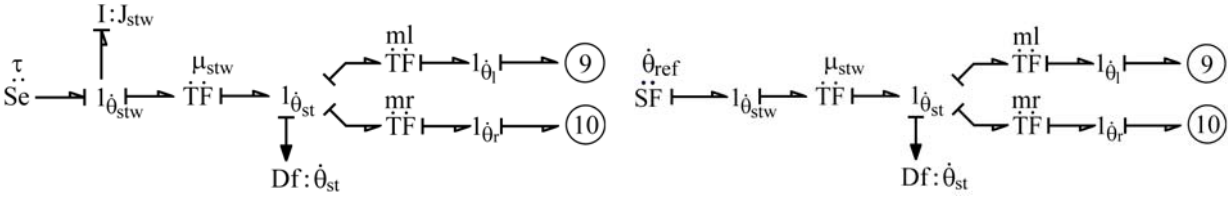

Fig. 17. Bond graph model of (a) Steering system; and (b) Modified steering system required for comparing vehicle's yaw rate with the test and simulation result given by Drozdz and Pacejka [24]

5. Simulation results for four wheel model

The normal loads or load transfer on the wheels vary due to pitch, yaw and roll motions. At high speeds, aerodynamic forces can as well affect the load transfer. Therefore, the load on each wheel, which is the deciding factor of maximum braking and driving torques, is influenced by various factors; broadly the operational conditions (speed, steering angle, ...) and the environmental conditions (wind speed, road condition, ...). The model parameters used in simulations for full vehicle model is given in Table 3.

Table 3. Parameter values of full vehicle.

Sub-system	Parameter values			
Vehicle body	m_c = 1600 kg	J_{cx} = 260 kg.m^2	J_{cy} = 1110 kg.m^2	J_{cz} = 1370 kg.m^2
	a = 0.9 m	b = 1.5 m	c = 0.7 m	h = 0.1 m
Suspension	K_{sx} = 10^7 N/m	R_{sx} = 2000 N.s/m	K_{sy} = 10^7 N/m	R_{sy} = 2000 N.s/m
	K_{sz} = 80 kN/m	R_{sz} = 500 N.s/m	K_{stx} = 10^7 Nm/rad	R_{stx} = 2000 N.m.s/rad
	K_{sty} = 0 Nm/rad	R_{sty} = 0 N.m.s/rad	K_{stz} = 10^6 Nm/rad	R_{stz} = 360 N.m.s/rad
Wheel	m_w = 15 kg	J_{wx} = 0.1 kg.m^2	J_{wy} = 0.2 kg.m^2	J_{wz} = 0.1 kg.m^2
	r_w = 0.3 m			
Tyre	K_t = 305 kN/m	R_t = 200 N.s/m		
	C_1 = 1.029	C_2 = 17.16	C_3 = 0.523	C_4 = 0.03
Brake	σ_{low} = 0.2	σ_{high} = 0.25	s_g = 0.01	k_g = 250 N.m
	r_{bd} = 0.15 m	R_{lm} = 0.04 N.s/m	K_{ca} = 10^4 N/m	K_{re} =10^6 N/m
	l_a = 1 m			
Steering wheel	J_{sw} = 1 kg.m^2	δ = 0.1 rad		

In the next step, the developed vehicle model is further validated by comparing the results with experimental maneuver data available in literature. Once the initial simulation is satisfactory, simulation of ABS was carried out using square pulse braking input. The pulse signal width is modulated for above instances to get the output. Then a comparative study between conventional braking and ABS is carried out. Finally, various simulations are performed to check the effectiveness of the controller from vehicle performance perspective. The simulations were conducted in Symbols software with the specifications given in Section 3.4.

5.1. Validation of four wheel model

The test data of [24] are used validate the developed four wheel model. In [24], slalom maneuver test was carried out on the vehicle at fixed vehicle speed of 50 km/h (13.88 m/s) and the steering wheel angle and the yaw rate were measured. The steering wheel angle was maintained between ± 100 degrees and the gear ratio between the steering wheel and axle rotation was 25:1. With this small change in axle orientations, the under-steered vehicle's linear speed remains almost constant at 50 km/h.

The experimental steering angle values (δ_{stw} in Fig. 18) at fixed time intervals were obtained from the graphs in [24] and were used as input ($\dot{\theta}_{ref} = d\delta_{stw}/dt$) in the developed four wheel bond graph model. The simulated yaw rates are compared with the experimentally obtained yaw rates of [24] in Fig. 18. Moreover, the

results obtained in [24] from a reduced order vehicle model are also plotted in Fig. 18 for comparison. It is found that the two models accurately predict the actual handling behaviour of the vehicle.

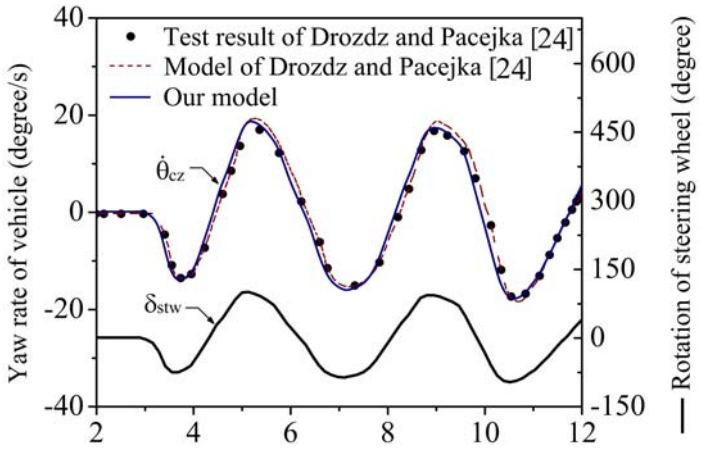

Fig. 18. Comparison of vehicle's yaw rate with the test and simulation results of [24] during slalom maneuver at vehicle speed of 50 km/h.

5.2. Anti–lock braking system in four wheel vehicle

Implementation of ABS has been carried out on the planar bicycle model to fine tune and test the control algorithm. Once the controller implementation (program) was found to be satisfactory, it was ported to the full vehicle model.

The vehicle was brought to a steady longitudinal velocity of 33.3 m/s (120 km/h) along a straight path and then the ABS was applied on the front wheels. The brake input signal as square pulse was simulated to get the ABS characteristic. Figure 19(a) shows how the variation in the rotational speed of the wheel and vehicle speed take place when ABS is operational in an emergency braking condition. Then the simple control logic, whose flow diagram is shown in Fig. 2(b), was implemented to maintain the slip ratio of the vehicle in the so called *sweet spot* of the friction-slip curve (Figs. 4 and 5) and the result in Fig. 19(b) shows that the slip ratio lies between the desired limits, i.e., 0.2 to 0.25. The maximum braking force required for ABS is 4988.28 N (Fig. 19(c)). The time taken for stopping the car is approximately 4.16s.

The brake system performance at different initial vehicle speeds was also tested through simulations. The results given in Fig. 20 are for dry asphalt road condition. It is seen that the time taken to bring the vehicle to a complete halt is 4.16s, 2.65s and 1.35s for initial vehicle speeds of 120 km/h, 80 km/h and 40 km/h, respectively. Although the curves in Fig. 20 look apparently parallel, they are not exactly parallel. This discrepancy is due to the non-linear nature of the slip-friction curve.

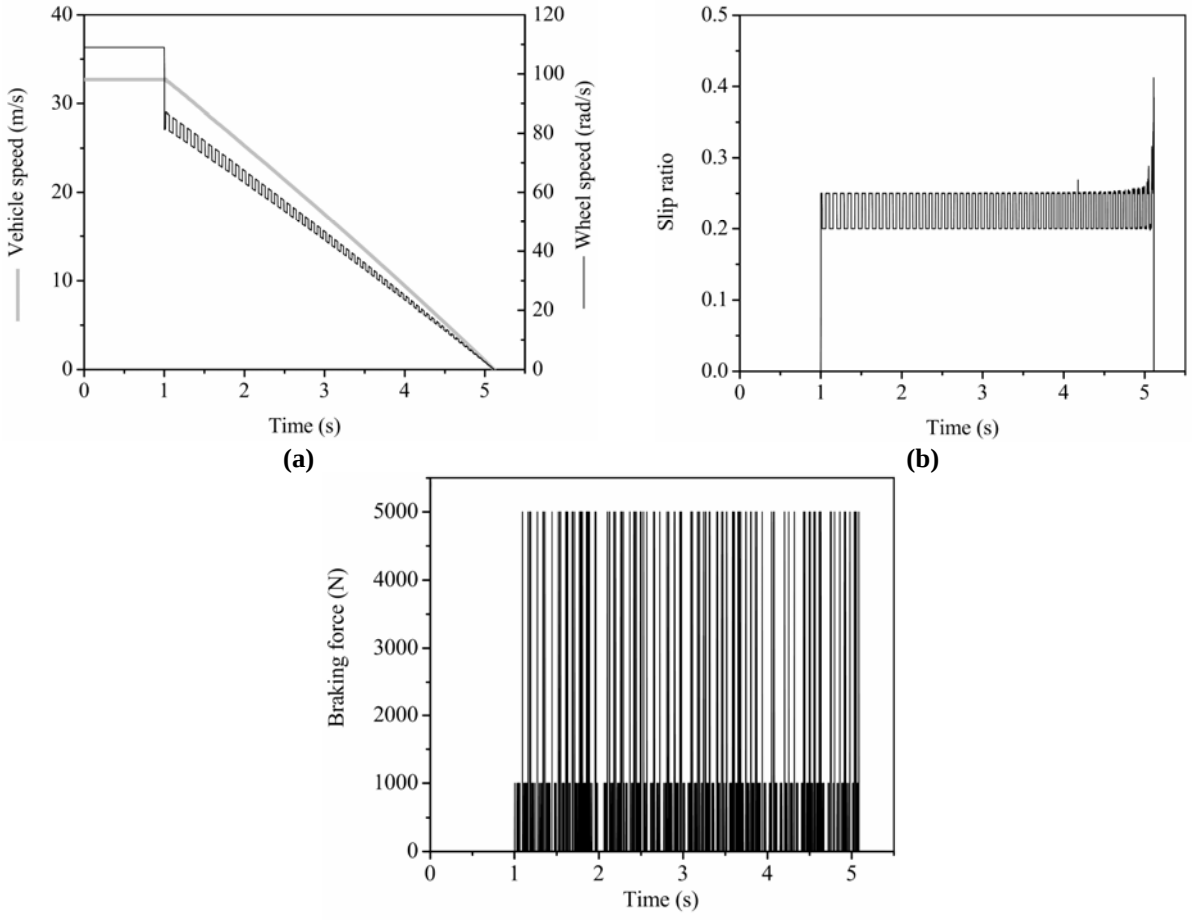

Fig. 19. (a) Vehicle and wheel speed; (b) Wheel slip ratio; and (c) Braking force during braking from 120 km/h.

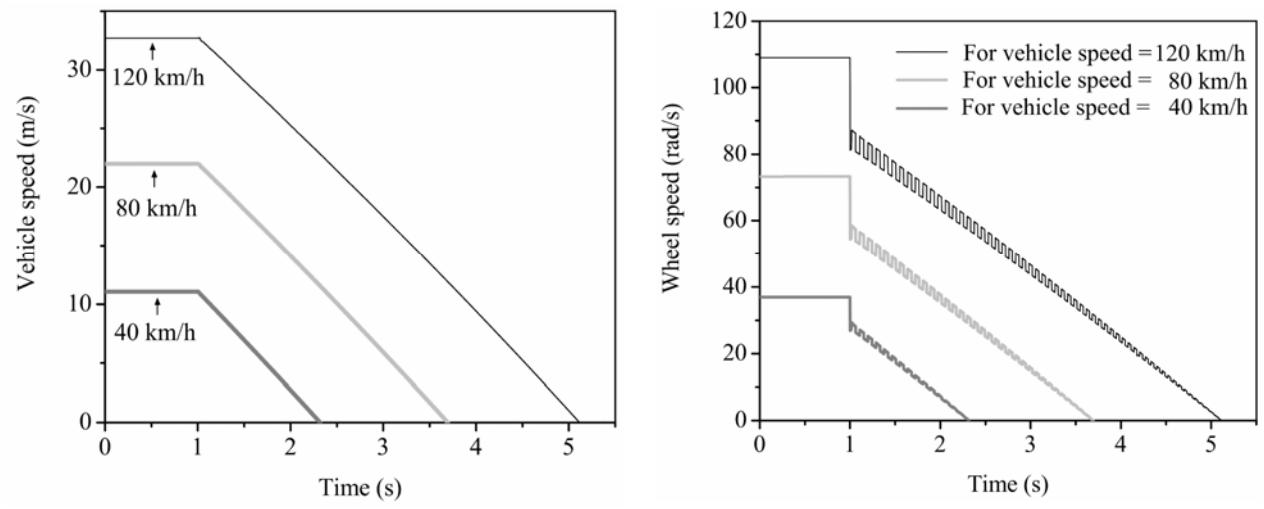

Fig. 20. (a) Vehicle and (b) wheel speed during ABS application at various initial vehicle speeds.

ABS is more useful in adverse driving conditions. A comparison of ABS performance for different road conditions is given in Fig. 21. It is found that the braking time increases as the friction coefficient reduces due to the road condition. The ABS actuation is clearly seen from the variations in wheel speed during braking (Fig. 21(b)). Specific parts of the wheel speed response are zoomed in Fig. 21(b) for closer inspection. There are insignificant variations in results for dry and wet asphalt road conditions. However, in snow driving condition, it is difficult to control the wheel slip due to lack of grip between the road and the tyre. While braking on snow, not only the stopping time is large as expected but also the switching frequency is large. This means that the ABS actuation has to be very fast in adverse braking conditions.

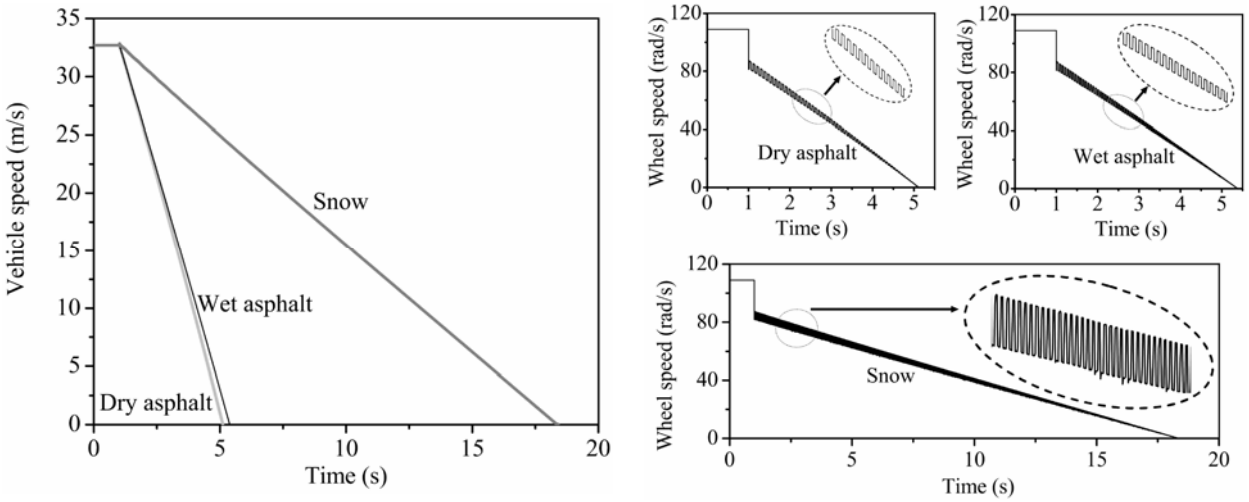

Fig. 21. (a) Vehicle and (b) wheel speed during braking from 120 km/h on various road surfaces.

The brake system design needs an integration of control system with the physical system model. Moreover, the brake system actuation rate is a factor to be taken into consideration during its design. The brake system is repeatedly used in city driving conditions where traffic is congested and often chaotic. Increase in longevity and reliability of brake system components may contribute towards improvement of the overall road safety standard and fewer accidents.

6. Conclusions

A detailed bond graph model of a vehicle with sub-models for its components, especially the braking system, has been developed in this paper. ABS controllers have been designed for the vehicle under consideration. The full vehicle model includes dynamics of the load transfer on the wheels while the vehicle makes a maneuver. The basic

scheme for ABS controller modelling, simulation and analysis to maintain the wheel slip within a desired range are presented. ABS was modeled using an equivalent mechanical braking system of the actual hydraulic system. The vehicle models and control algorithms have been comprehensively validated by comparing the simulation results with experimental and numerical results available in the literature.

The model and the algorithm developed here for controller design are good enough to take care of different road and operating conditions. Moreover, the bond graph approach being a multi-disciplinary modelling tool makes it convenient to integrate models in other energy domains such as electrical drives and fuel cells into the developed bond graph model. It found from simulation studies that the ABS actuation rate needs to be extremely fast in adverse driving conditions. The actuation rate and peak brake force *etc.* are to be considered during mechanical design of the brake system actuator so that desired maximum forces, actuator response time *etc.* are achieved while proper care is taken to increase the fatigue life of brake system components and reduce the wear in the brake pads. The reconfigurable simulation model developed in this article in which vehicle and brake system parameters can be changed serves as a design and controller prototyping platform. This integrated physical and control system model avoids expensive field trials during early stages of brake system control law tuning and actuator sizing.

References

[1] D.C. Karnopp, D.L. Margolis, R.C. Rosenberg, System Dynamics, Modeling and Simulation of Mechatronic Systems, John Wiley & Sons, NY , 2000.

[2] A. Mukherjee, R. Karmakar, A.K. Samantaray, Bond Graph in Modeling, Simulation and fault Identification, CRC Press, FL, 2006.

[3] W. Borutzky, Bond Graphs-A Methodology for Modelling Multidisciplinary Dynamic Systems, SCS Publishing House, Erlangen, San Diego, 2004.

[4] A.K. Samantaray, B. Ould-Bouamama, Model-based Process Supervision, Springer Verlag, London, 2008.

[5] A.M. Bos, Modeling Multibody Systems in terms of Multibond Graphs, with application to a motorcycle, PhD thesis at Twente Univ., 1986.

[6] W. Cho, A Bond Graph Approach to the Modeling of General Multibody Dynamics Systems, KEME International Journal 12 (5) (1998) 888–898.

[7] P.J. Gawthrop, Physical model-based control: A bond graph approach, Journal of the Franklin Institute 332 (3) (1995) 285–305.

[8] G. Dauphin-Tanguy, A. Rahmani, C. Sueur, Bond graph aided design of controlled systems, Simulation Practice and Theory 7 (5–6) (1999) 493–513.

[9] P.M. Pathak, R.P. Kumar, A. Mukherjee, A. Dasgupta, A scheme for robust trajectory control of space robots, Simulation Modelling Practice and Theory 16 (9) (2008) 1337–1349.

[10] R.F. Ngwompo, P.J. Gawthrop, Bond graph-based simulation of non-linear inverse systems using physical performance specifications, Journal of the Franklin Institute 336(8) (1999) 1225–1247.

[11] P.J. Gawthrop, Bond graphs: A representation for mechatronic systems, Mechatronics 1 (2) (1991) 127–156.

[12] J.J. Granda, The role of bond graph modeling and simulation in mechatronics systems: An integrated software tool: CAMP-G, MATLAB–SIMULINK, Mechatronics 12 (9-10) (2002) 1271–1295.

[13] D. Hrovat, J. Asgari, M. Fodor, Automotive Mechatronic Systems, in: Mechatronic Systems Techniques and Applications, Volume 2, Gordon and Breach Science Publishers, Amsterdam (2000) 1–98.

[14] G. Filippini, N. Nigro, S. Junco, Vehicle dynamics simulation using bond graphs, International conference on Integrated modelling and analysis in applied control and automation (IMAACA 2007), Buenos Aires, Argentina.

[15] D. Margolis, T. Shim, A bond graph model incorporating sensors, actuators, and vehicle dynamics for developing controllers for vehicle safety, Journal of the Franklin Institute 338 (2001) 21–34.

[16] H.B. Pacejka, Modelling Complex Vehicle Systems Using Bond Graphs, Journal of the Franklin Institute 319 (1/2) (1985) 67–81.

[17] L.S. Louca, J.L. Stein, D.G. Rideout, Generating Proper Integrated Dynamic Models for Vehicle Mobility Using a Bond Graph Formulation, Proceedings of the 2001 International conference on Bond Graph Modeling (ICBGM'01) , Phoenix, AZ 33(1) (2001) 339–345.

[18] H.B. Pacejka, Tyre and Vehicle Dynamics, Butterworth-Heinemann, Elsevier, UK, 2006.

[19] Y. Oniz, E. Kayacan, O. Kaynak, A Dynamic Method to Forecast the Wheel Slip for Antilock Braking System and its Experimental Evaluation, IEEE transactions on systems, man, and cybernetics part B cybernetics 39 (2) (2009) 551–560.

[20] R.G. Longoria, A. Al-Sharif, C.B. Patil, Scaled vehicle system dynamics and control: a case study in anti-lock braking, Int. J. Vehicle Autonomous Systems 2 (1/2) (2004) 18–39.

[21] M. Oudghiri, M. Chadli, A.E. Hajjaji, Robust Fuzzy Sliding Mode Control for Antilock Braking system, Int. Journal on Sciences and Techniques of Automatic control 1 (1) (2007) 13–28.

[22] C.B. Patil, R.G. Longoria, J. Limroth, Control prototyping for an Anti-lock braking control system on a scaled vehicle, in: proceedings of 42nd IEEE Conference on decision and control, USA (2003) 4962–4967.

[23] G.F. Mauer, A fuzzy logic controller for an ABS braking system, IEEE transactions on fuzzy systems 3 (4) (2005) 381–388.

[24] W. Drozdz, H.B. Pacejka, Development and Validation of a Bond Graph Handling Model of an Automobile, Journal of the Franklin Institute 328 (5/6) (1991) 941–957.

[25] R. Merzouki, B. Ould-Bouamama, , M.A. Djeziri, M. Bouteldja, Modelling and estimation of tire–road longitudinal impact efforts using bond graph approach, Mechatronics 17 (2-3) (2007) 93–108.

[26] S.L. Koo, H.S. Tan, M. Tomizuka, An Improved Tire Model for Vehicle Lateral Dynamics and Control, in: proceedings of the American Control Conference, Minneapolis, Minnesota, USA, 2006, pp. 5879–5884.

[27] R. Rajamani, Vehicle dynamics and control, Springer, US, 2006.

[28] B. Ozdalyan, Development of a slip control anti-lock braking system model, International Journal of Automotive Technology 9 (1) (2008) 71–80.

[29] K. Li, J.A. Misener, K. Hedrick, On-board road condition monitoring system using slip-based tyre–road friction estimation and wheel speed signal analysis, J. Multi-body Dynamics, IMechE 221 (2007) 129–146.

[30] M. Denny, The dynamics of antilock brake systems, European Journal of Physics 26 (2005) 1007–1016.

[31] T.D. Gillespie, Fundamentals of Vehicle Dynamics, SAE International, 1992.

[32] H.K. Fathy, Z.S. Filipi, J. Hagena, J.L. Stein, Review of hardware-in-the-loop simulation and its prospects in the automotive area, Proceedings of SPIE-The international Society for Optical Engineering 6228 (2006) 62280E.1–62280E.20.

[33] M.L. Kuang, M. Fodor, D. Hrovat, M. Tran, Hydraulic Brake System Modeling and Control For Active Control of Vehicle Dynamics, in: proceedings of the American Control Conference, San Diego, California, 1999, pp. 4538–4542.

[34] S. Drakunov, U. Ozguner, P. Dix, B. Ashrafi, ABS Control Using Optimum Search via Sliding Modes, IEEE Transactions on Control Systems Technology 3 (1) (1995) 79–85.

[35] A. Sanyal, R. Karmakar, Directional stability of Truck-Dolly-Trailer System, Vehicle System Dynamics 24 (8) (1995) 617–637.

[36] T. Ersal, H.K. Fathy, J.L. Stein, Structural simplification of modular bond-graph models based on junction inactivity, Simulation Modelling Practice and Theory 17 (2009) 175–196.

[37] Symbols User's manual, HighTech Consultants, http://www.htcinfo.com.

[38] B. Ould Bouamama, K. Medjaher, A.K. Samantaray, M., Staroswiecki, Supervision of an industrial steam generator. Part I: Bond graph modeling, Control Engineering Practice 14 (2006), 71–83.

[39] A.K. Samantaray, K. Medjaher, B. Ould Bouamama, M. Staroswiecki, G. Dauphin-Tanguy, Diagnostic bond graphs for online fault detection and isolation, Simulation Modelling Practice and Theory 14 (2006), 237–262.

[40] B. Ould Bouamama, Bond graph approach as analysis tool in thermofluid model library conception, Journal of the Franklin Institute 340 (2003), 1–25.

[41] H.T. Szostak, W.R. Allen, T.J. Rosenthal, Analytical Modeling of Driver Response in Crash Avoidance Maneuvering. Volume II: An Interactive Model for Driver/Vehicle Simulation, U.S Department of Transportation Report NHTSA DOT HS-807-271 (1988).

[42] K. Huh, D.Hong, J.L. Stein, Development of A Lane Departure Monitoring and Control System, Journal of Mechanical Science and Technology 19 (11) (2005) 1998–2006.